








N.V. Khan^{1*} , M. Baláž² , M.M. Burkitbayev¹ ,
 B.B Tatykayev¹ , Zh.S. Shalabayev³ , A.I. Niyazbayeva¹ ,
 F.Kh. Urakaev^{1,4} 

¹Al-Farabi Kazakh National University, Almaty, Kazakhstan

²Institute of Geotechnics, Košice, Slovakia

³Scientific Center of Anti-infectious Drugs, Almaty, Kazakhstan

⁴Sobolev Institute of Geology and Mineralogy, Novosibirsk, Russia

*e-mail: Natalya.Khan@kaznu.edu.kz

(Received 2 May 2022; received in revised form 17 May 2022; accepted 07 June 2022)

Solvothermal DMSO-mediated synthesis of the S/AgI microstructures and their testing as photocatalysts and biological agents

Abstract. S/AgI microstructures were produced by solvothermal DMSO-mediated synthesis using two methods of sulfur precipitation: at room temperature (method 1) and by water (method 2). The samples were obtained with different percentages of AgI: 10, 30 and 50 %. Microstructures were investigated with help of XRD, Raman spectroscopy and SEM/EDS (elemental mapping). XRD and Raman spectroscopy confirmed the presence of sulfur and AgI. EDS elemental mapping revealed that samples were composed of large grains of sulfur covered by smaller grains of AgI. The obtained SEM micrographs revealed that the 1st method gave larger grains of sulfur in comparison with the 2nd method. Testing of the microstructures as photocatalysts showed the low activity; as the prepared samples were able to degrade no more than 7 % of the molecules of Orange II. Significant biological activity was detected only for S/AgI (2) 50 % sample, as it was able to suppress test strains of *S. aureus* ATCC BAA-39, *P.aeruginosa* ATCC 9027 and *Erwinia amylovora* at MBC/MFC 5000 µg/mL, and *E. coli* ATCC 8739 at 2500 µg/mL.

Key words: sulfur; silver iodide; solvothermal synthesis; microstructures; photocatalytic activity; biological activity.

Introduction

Micro- and nano-structures are widely used in various fields [1-3]. Among them are structures based on sulfur and silver iodide (AgI) [4, 5]. The necessity of obtaining such structures is explained by the possibility of their application in photocatalysis, biochemistry and electrochemistry. The production of silver halides is caused by high cost of the feedstock, so the question arises of using cheaper accompanying components that could enhance certain properties and reduce the amount of used silver halide. Sulfur can potentially serve as such a cheap and accessible component.

Sulfur is an inorganic substance, which used in wide range of the science and technology [6]. It is often used in production of batteries, because of its semiconductor properties [7, 8]; in drugs production because of its anti-inflammatory properties and the ability to treat different diseases

[6, 9]. In the production of fertilizers, sulfur used in oxidized form, which improves the ability of plants to absorb the necessary components [10]; in the production of antibacterial and antifungal agents, sulfur is more active in nano-state [11, 12]. Sulfur is also used in photocatalytic CO₂-reduction [13] and hydrogen evolution [14] in combination with C₃N₄. For degradation of organic dyes, sulfur doping by ZnO and PbO is also used [15, 12].

AgI is inorganic substance with specific properties. The most common application of the AgI is photocatalysis [16-22] because of its photosensitivity. In degradation of model solutions and various contaminants, AgI is used with other materials for obtaining of the enhanced properties. For example, it can be TiO₂, Ag, Bi₅O₇I, BiOI, C₃N₄, SnS₂ and others [17-19]. Another application field of AgI is microbiology, more accurately, the production of antimicrobial agents [13, 17-19, 21]. Here AgI

also used in combinations with other substances, like, PVA, ZnO and chlorophyll [18].

Preparation methods of above mentioned materials encompass mainly from hydrothermal to solid-phase route [6-15, 20-24]. In our case, we have chosen the solvothermal DMSO-mediated method of synthesis. DMSO is aprotic and bipolar solvent, which is used in medicine, biotechnologies, chemistry and other fields [25]. DMSO is less dangerous and toxic in comparison with other aprotic and polar organic solvents; it can serve as a source of sulfur and dilute a big number of substances [26-28]. Our research group have already studied the behavior and solubility of the sulfur in DMSO media [29] and synthesized sulfur-containing materials with silver compounds [30, 31]. In the present case, we have used similar methodology to [30], however, the mass ratios of the components was changed and in the process of precipitation of sulfur by water, the volume of it was different. Hence, this research work is devoted to the synthesis of microstructures based on sulfur and AgI, and further study of the effect of the method of obtaining and the percentage of components on the manifestation of photocatalytic and biological activities.

Materials and methods

Materials. Silver nitrate, ammonia iodide, sulfur, Orange II were provided by Sigma Aldrich (Germany). Dimethyl sulfoxide and sodium chloride were supplied by OJSC Mikhailovsky Plant of Chemical Reagents (Russia). Mueller Hinton Agar (M173) and Mueller Hinton Broth (M391) were purchased from HiMedia (India). All reagents were of analytical grade and deionized water was used in experiments.

Characterization. X-ray diffraction (XRD) was used for determination of the phase composition of the samples. Analysis was conducted with Rigaku MiniFlex 600 X-ray diffractometer using copper radiation ($\lambda = 0.15405$ nm). The XRD patterns were processed with help of the ICCD-PDF2 release 2016 database.

Raman spectroscopy was conducted for identification of the samples composition and proving the XRD results. Analysis was made on Solver Spectrum (NT MDT Instruments, Russia) spectrometer using an 1800/500 diffraction grating.

The morphology and size of the particles were studied by scanning electron microscopy (SEM) and particle distribution by Energy Dispersive X-ray mapping analysis (EDS mapping). Analysis was conducted on Quanta 200i 3D microscope (FEI,

Netherlands). The analyses were conducted in the NNLOT laboratory of al-Farabi Kazakh National University.

Absorption spectra of the samples were obtained with help of SF-56 (OKB Spektr, Russia) spectrophotometer, using wavelength range from 350 to 700 nm.

Synthesis of the S/AgI microstructures (sulfur deposition at room temperature), (1) The process of the synthesis was conducted with using an apparatus, which consist of three-neck round bottomed flask, thermometer, backflow condenser and magnetic stirrer. The similar procedure was used in [30]. For obtaining silver iodide, the solutions of AgNO_3 and NH_4I in DMSO were used (50 mL of each solution). The required amount of sulfur was dissolved in 100 ml of DMSO at 120 °C with constant stirring. Then 1/10 part of the NH_4I was added drop by drop to the reaction mixture and the content of the flask was stirred for 15 minutes. After that, a solution of AgNO_3 and NH_4I were introduced into the flask alternately, drop by drop. Thus, AgI is formed because of the ion exchange reaction (1). Then, the resulting mixture was cooled at room temperature for 12 hours for complete precipitation of sulfur from the DMSO solution. Further, the mixture was stirred and precipitated in a centrifuge (Rotina 380, Hettich, Germany) (4000 rpm, 10 min), washed 2 times with deionized water and dried for 12-14 hours, at 70 °C.



The marking of the samples depending on the content of AgI and synthesis method was adopted as follows: S/AgI (1) 10, 30, 50 % and S/AgI (2) 10, 30, 50 %. Here 10, 30, 50 % shows the content of AgI, the rest is sulfur, (1) – a synthesis method in which sulfur precipitates at room temperature and (2) – a synthesis method in which sulfur precipitates by diluting the reaction mixture with water.

Synthesis of the S/AgI microstructures (sulfur deposition by water), (2) The initial steps of synthesis were identical to the previous method described above. However, the process of the precipitation of sulfur was different. After adding solutions of AgNO_3 and NH_4I to the flask, deionized water was poured into the mixture. The volume ratio of water to the reaction mixture was 1:1. At final step, the products were precipitated, washed and dried.

Synthesis of pure AgI. The procedure of obtaining of pure AgI was the same as the previous, but the step of introducing of sulfur to the reaction mixture was excepted.

Synthesis of pure S. The procedure of obtaining of pure S was the same as the previous, but the step of introducing of solutions of AgNO_3 and NH_4I to the reaction mixture was skipped.

Photocatalytic activity. 20 mg of the microstructure was introduced to 40 mL of the Orange II (10 mg/L). For uniform distribution of the sample in the volume of the solution, ultrasound treatment was used (3 min). To stabilize the samples, the adsorption-desorption test was conducted in the dark conditions for 1 hour (the sample was covered with aluminum foil). When the adsorption process is complete and the sample is stable, the visible light exposure begins. The source of visible light was a 300 W Osram Vita-lux lamp equipped with a UV filter. The irradiation intensity was 15 mW/cm^2 . Sampling was carried out every 30 minutes. Then, the sample was centrifuged (Rotina Micro 200, Hettich, Germany) for 3 min at 10000 rpm. The photocatalytic activity of the samples was studied with help of UV-Vis spectrophotometer. Each study was conducted twice to confirm the results.

Biological activity. For study of the biological activity the following bacterial strains of American Type Culture Collection (ATCC) were used: *Staphylococcus aureus* ATCC 6538-P (collection sensitive strain); *Candida albicans* ATCC 10231 (collection sensitive strain); *Escherichia coli* ATCC 8739 (collection sensitive strain); *Pseudomonas aeruginosa* ATCC 9027 (collection sensitive strain); *Erwinia amylovora* (phytopathogenic strain), *Staphylococcus aureus* (subsp. aureus) ATCC BAA-39 and *Escherichia coli* ATCC BAA-196TM. The sensitivity of microorganisms was studied on standard nutrient media [32].

Preparation of bacterial suspension. For preparation of the bacterial solution 5 mL of saline solution was poured to the test tube, then the test strain was added, and vigorously stirred. The result suspension was tested for the following characteristics: for bacteria, the turbidity was 0.5 McFarland units (which corresponds to a concentration of 1.5×10^8 CFU/mL); for yeast – like fungi, the turbidity was 2.5 (which corresponds to a concentration of 7.5×10^8 CFU/mL). 1 mL of the suspension was transferred in 9 mL of sterile saline solution for tenfold dilutions. As a result, a concentration of 1.5×10^6 CFU/mL for bacteria and 7.5×10^6 CFU/mL for yeast-like fungi, was obtained. The purity of bacterial strains was examined before each experiment.

Method of two-fold serial dilutions. The biological activity was studied on water suspensions of microstructures (10 mg/mL).

In typical experiment, 0.5 mL of Muller-Hinton broth was poured to the plate with 48 wells. Then, 0.5 mL of the water solution of microstructure was poured in the first well of the row and stirred. Hence, 1:1 dilution was obtained. For 1:2 dilution, 0.5 mL of mixture from the first well was stirred and transferred to the second well. In that way other two-fold serial dilutions up to 1:128 were prepared. After that, 0.05 mL of test strains of microorganisms were added to all wells. For each series of dilutions, medium control and strain growth control were used. Experimental procedures were carried out in two repetitions for all samples [32, 33].

The incubation of the samples was conducted for 48 hours at a temperature of $(22 \pm 1)^\circ\text{C}$ for fungi and for 18-24 hours at $(37 \pm 1)^\circ\text{C}$ for bacteria. The seeding at Petri dish was carried out to determine the number of living cells. The incubation conditions were similar to conditions described above.

The biological activity was determined by examining the visible growth of microorganisms on the surface of a solid nutrient medium. The minimal bactericidal (fungicidal) concentration (MBC or MFC) was considered as a measure of the biological activity.

All experiments were performed in three repetitions.

Results and discussion

XRD analysis. In the Figure 1 the XRD patterns of the S/AgI (1, 2) 10, 30, 50 %, pure AgI and S (1, 2) are shown. According to the obtained results there are three noticeable peaks of AgI at 23.76 , 39.24 and 46.36° , which correspond to its gamma modification. Also, with an increase in the content of AgI, the intensity of these peaks increases. As for sulfur, it can be seen that samples represented by one clear peak at about 23.18° and small peaks in the range between 25 and 30° . There is also an increase in the intensity of peaks, with an increase in the sulfur content in the samples. In order to confirm the presence of identified phases, the Raman spectroscopy measurements have been conducted.

Raman spectroscopy. In the Figure 2 the Raman spectra of S/AgI (1, 2) 10, 20, 50 %, pure AgI and S (1, 2) are shown. Pure AgI (orange spectrum) is represented by two peaks at 74 and 109 cm^{-1} , while pure sulfur (red and blue spectra) has four clear peaks at 89 , 158 , 223 and 477 cm^{-1} . The obtained results correspond to the [34]. The signals corresponding to both phases could be identified in S/AgI. Hence, synthesized samples contain both S and AgI.

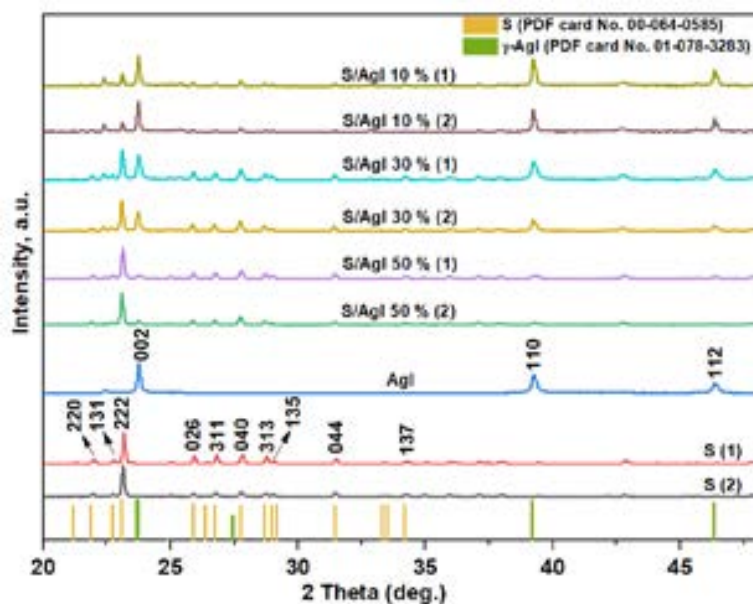


Figure 1 – XRD patterns the S/AgI (1, 2) 10, 30, 50%, AgI and S (1, 2)

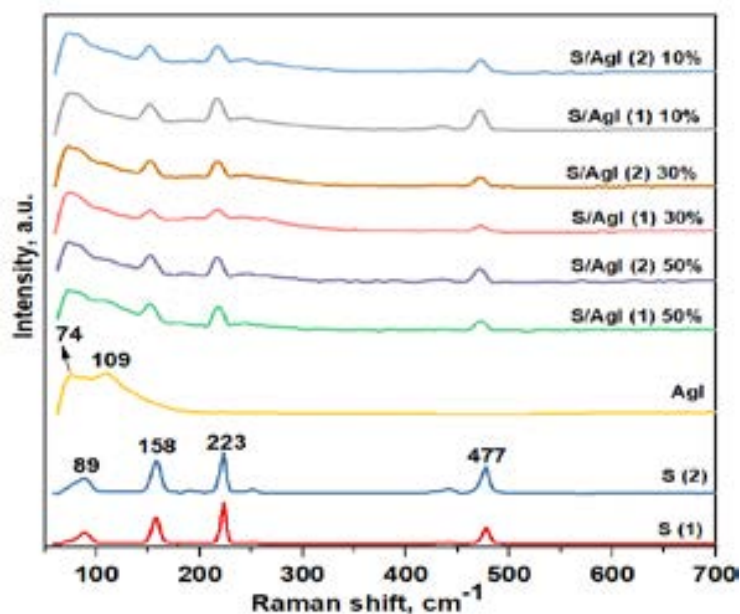


Figure 2 – Raman spectra of the S/AgI (1, 2) 10, 30, 50 %, AgI and S (1, 2)

SEM/EDS analyses. For understanding of distribution of all components of the samples the EDX mapping have been conducted. For this analysis only 50 % samples were analyzed, because the samples with a higher sulfur content melted.

In Figure 3 (a-h), the results for S/AgI (1, 2) 50 % are shown. In the case of S/AgI (1) 50 % sample, large sulfur grains were detected (Figure 3a). However, the small grains of sulfur also can be seen (Figure 3 b). As for Ag and I – it is evenly distributed

on the surface of the sulfur particles. Thus, the large grains of the sulfur are covered by a layer of the AgI [31]. For S/AgI (2) 50 % the presence of large grains

was not evidenced. In general, more homogeneous distribution of all elements was detected for this samples.

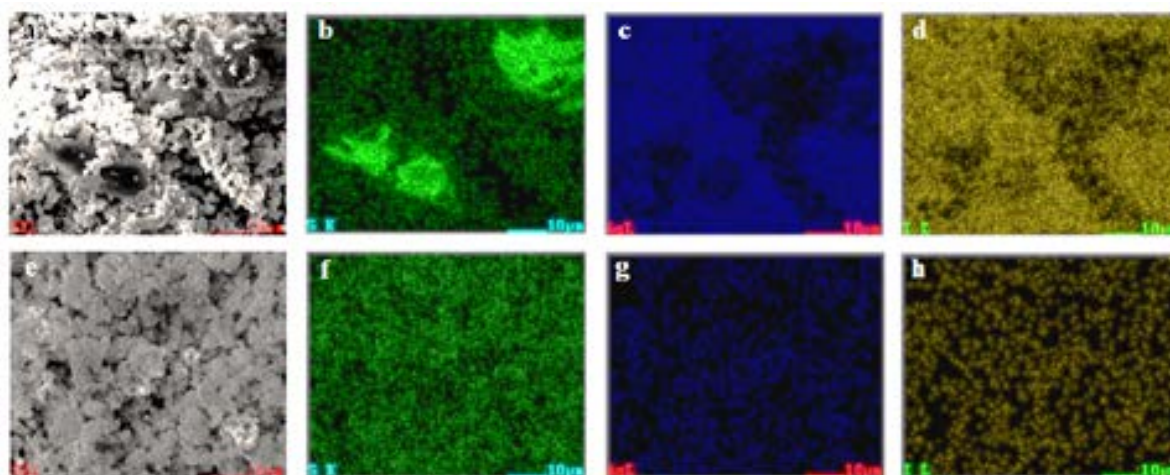


Figure 3 – EDS mapping of S/AgI 50% (1) (a-d), (2) (e-h). a, e – EDS layered images; b, f – EDS image of S distribution; c, g – EDS image of Ag distribution; d, h – EDS image of I distribution

To further confirm the presence of small AgI particles on the surface of sulfur grains, a more detailed SEM analysis was performed (Figures 4 – 6). In general, the presence of big particles covered by smaller ones can be seen in all samples. It is highly probable that sulfur is represented by dark large particles with irregular form and AgI by small light particles with even and clear boundaries.

The results of SEM analysis of S/AgI (1) 10 % are shown in the Figure 4 (a – c) and of S/AgI (2) 10% – in the Figure 4 (d – f). Here the first method gives the largest grains of the sulfur. The average size of sulfur in the S/AgI (1) 10 % is fluctuated from 20 to 50 μm , while for the S/AgI (2) 10 % it has size range from 10 to 20 μm . AgI particles obtained by method 1 have clear and smooth triangle and hexagonal form with the average size of 0.5 – 3 μm . AgI particles in the S/AgI (2) 10 % are irregular with size from 0.3 to 0.9 μm .

In Figure 5, 6 (a –f) the SEM of the S/AgI (1, 2) 30, 50 % are given. Here also the 1st method gave sulfur with bigger size in comparison to the 2nd method. The morphology and the size of the sulfur is similar to the samples with 10 % AgI content. The AgI particles obtained by method 1 have also triangular and hexagonal form with smooth surface

and in the method 2 the AgI particles exhibit irregular shape with loose surface. The size of AgI in the S/AgI (1) 30 % is in the range from 0.2 to 0.6 μm and for S/AgI (2) 30 % from 0.4 to 1 μm . In 50 % samples the 1st method produced sulfur particles with the size range from 20 to 50 μm and the 2nd method – from 5 to 10 μm . AgI grains are represented by size from 1 to 3 μm and from 0.5 to 2 μm for both method 1 and 2, respectively.

For easier perception of the data on the particle sizes of microstructures, we have given all the data in Table 1.

Photocatalytic activity. Figure 7a shows a comparison of the photocatalytic activity of the S/AgI (1, 2) 10, 30, 50 % micro-structures and pure AgI and S (1, 2). The results show that pure AgI is able to degrade 99% molecules of Orange II after 180 minutes of exposure to visible light, while after the same duration, the S/AgI (1, 2) samples of all compositions and pure sulfur do not show photodegradation higher than 7 %. Hence, the synthesized microstructures do not possess photocatalytic activity. Such result can be explained by the micro-size of the sulfur, which probably passivates otherwise photocatalytically active AgI. Maybe the higher content of the AgI could solve this problem.

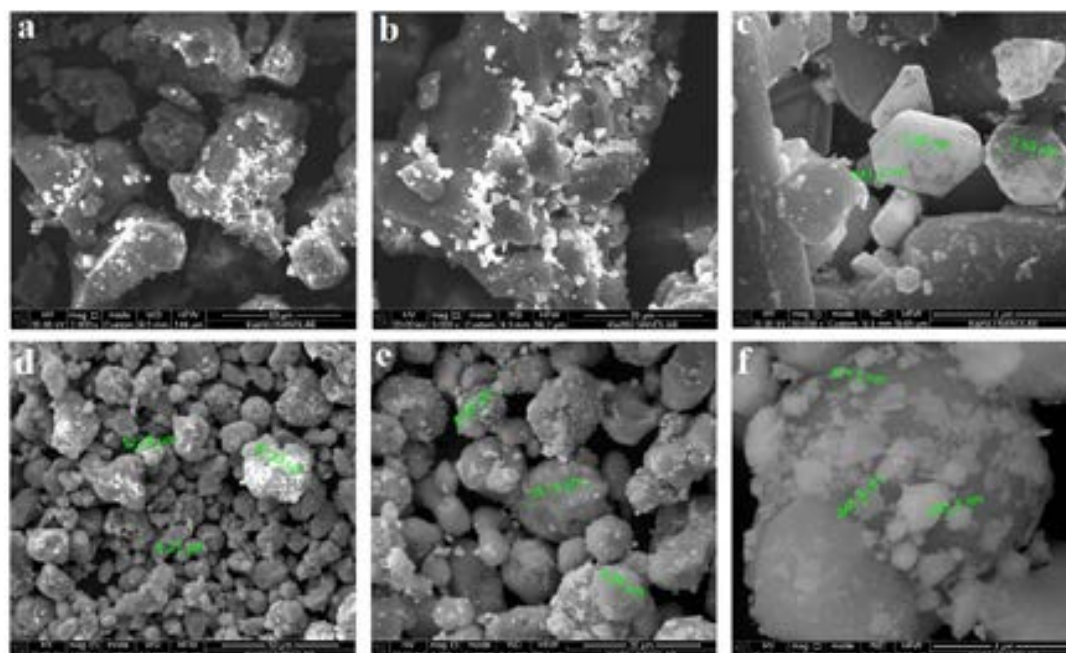


Figure 4 – SEM analysis of the: S/AgI (1) 10 % (a – 2000x; b – 5000x, c – 30000x magnification); S/AgI (2) 10 % (d – 2000x; e – 5000x, f – 30000x magnification)

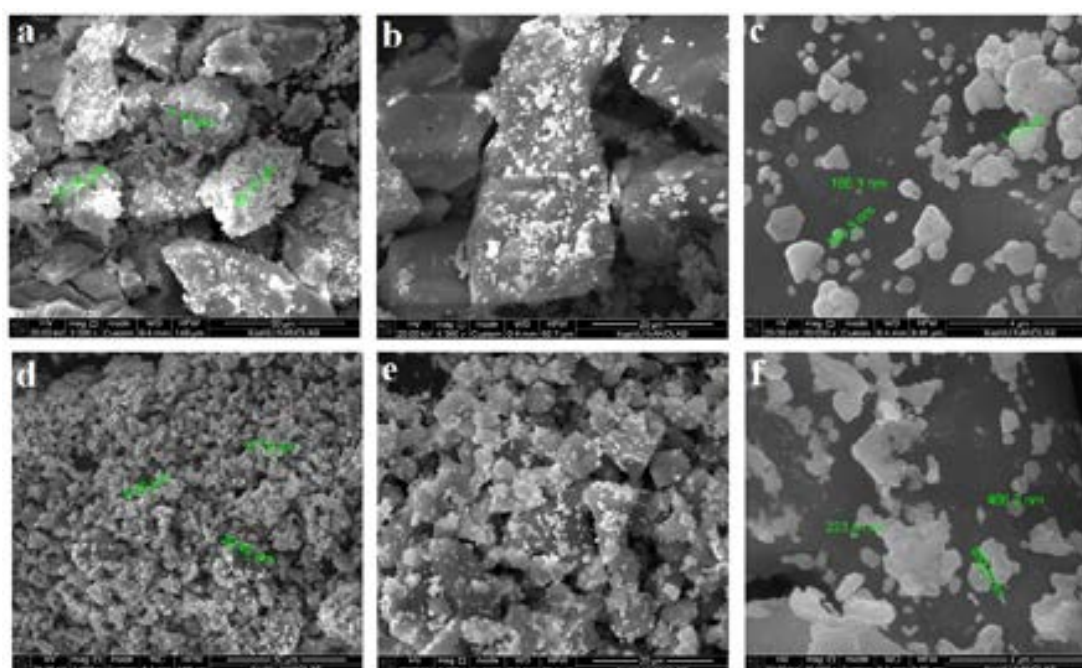


Figure 5 – SEM analysis of the: S/AgI (1) 30 % (a – 2000x; b – 5000x, c – 30000x magnification); S/AgI (2) 30 % (d – 2000x; e – 5000x, f – 30000x magnification)

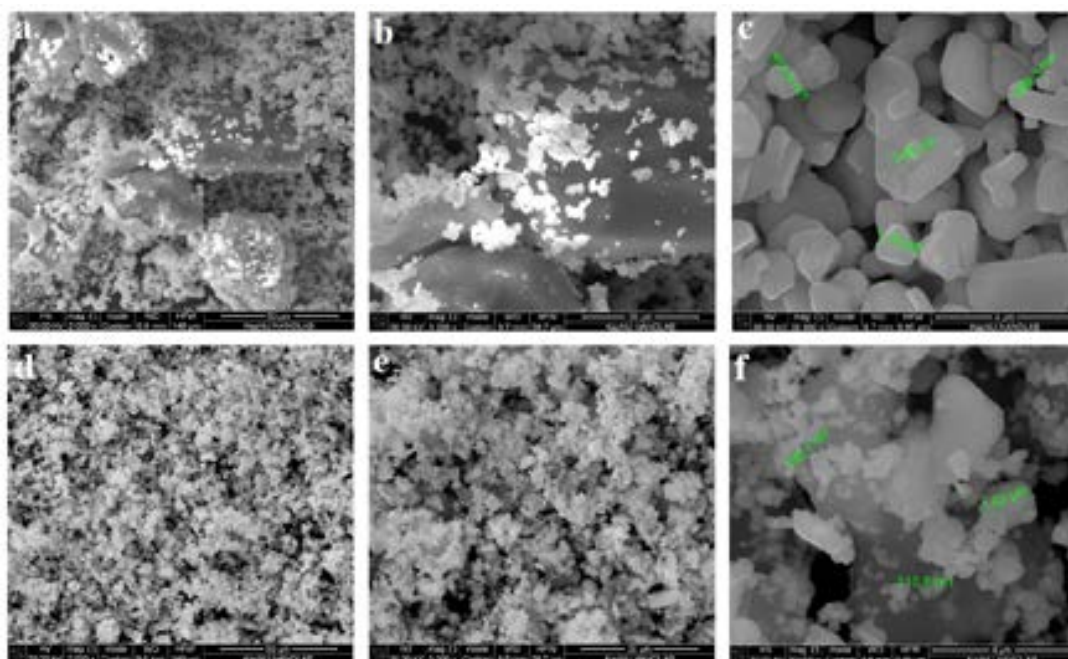


Figure 6 – SEM analysis of the: S/AgI (1) 50 % (a – 2000x; b – 5000x, c – 30000x magnification); S/AgI (2) 50 % (d – 2000x; e – 5000x, f – 30000x magnification)

Table 1 – The size ranges of the microstructures

Microstructure	The size range of the sulfur, μm	The size range of the AgI, μm
S/AgI (1) 10 %	20-50	0.5-3.0
S/AgI (2) 10 %	10-20	0.3-0.9
S/AgI (1) 30 %	20-50	0.2-0.3
S/AgI (2) 30 %	5-10	0.4-1.0
S/AgI (1) 50 %	20-50	1.0-3.0
S/AgI (2) 50 %	5-10	0.5-2.0

The kinetics of the photocatalytic process was accepted as a pseudo-first-order reaction: $\ln(C_0/C) = kt$. C_0 and C are initial and final concentrations, respectively, of model solution in moment of time t ; k (min^{-1}) is the rate constant of the photocatalytic reaction [35]. Other kinetics models were also studied, but the most suitable one was the pseudo-first-order reaction. The k

was found from the linear graphs. High Pearson's correlation coefficient r was a proof of the kinetic order of model solution degradation. Figure 8 b shows the pseudo-first order kinetics for photocatalytic degradation of Orange II by S/AgI (1, 2) 10, 30, 50 % microstructures. In the Table 2, the values of k and r for all synthesized samples can be found.

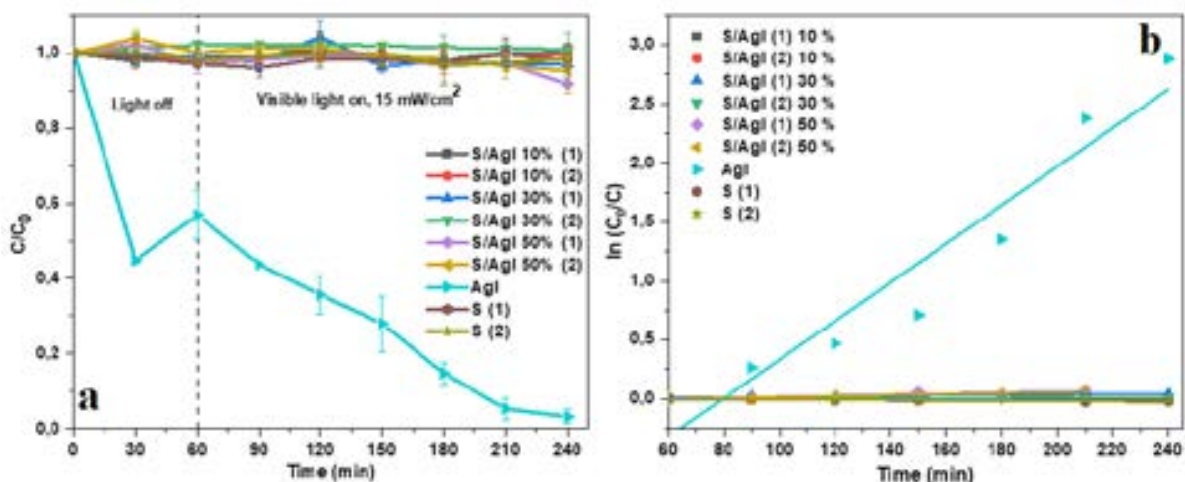


Figure 7 – Photocatalytic degradation of Orange II: a – comparison of the photocatalytic activity of the S/AgI (1, 2) 10, 30, 50 %, pure sulfur and AgI; b – Pseudo-first-order kinetics for photocatalytic degradation of the Orange II by all samples

Table 2 – Pseudo-first order rate constants of photocatalytic degradation of the Orange II for all samples

Sample	The rate constant, $k \cdot 10^2 \text{ min}^{-1}$	Pearson's coefficient, r
S/AgI (1) 10 %	0.006	0.974
S/AgI (2) 10 %	0.008	0.912
S/AgI (1) 30 %	0.019	0.911
S/AgI (2) 30 %	0.006	0.957
S/AgI (1) 50 %	0.046	0.983
S/AgI (2) 50 %	0.044	0.981
AgI	1.638	0.961
S (1)	0.001	0.898
S (2)	0.001	0.867

Biological activity. The resistance of the microstructures to microorganisms was measured relying on the MBC (MFC). The MBC (MFC) values were calculated from the dilutions. As concentration of the water suspensions of the samples was 10 mg/mL (10000 $\mu\text{g/mL}$), the calculations were done by the next scheme: 1:1 dilution corresponds to 5000 $\mu\text{g/mL}$, 1:2 dilution corresponds to 2500 $\mu\text{g/mL}$ and etc. These calculations were performed for all formulations and all dilutions (from 1:1 to 1:128). According to the study, pure substances and microstructures of all compositions did not show the ability to suppress microorganisms, only S/AgI (2) 50 % was active. It was able to suppress *S. aureus* ATCC

BAA-39, *P.aeruginosa* ATCC 9027 and *Erwinia amylovora* at MBC/MFC 5000 $\mu\text{g/mL}$. As for *E. coli* ATCC 8739, the S/AgI (2) 50 % was effective at 2500 $\mu\text{g/mL}$. Such results may indicate that there is a bond between sulfur and AgI, which leads to the manifestation of biological activity. This percentage ratio and the method of obtaining were the optimal conditions for this system. The results indicate the need for further investigation of the synthesis conditions and their effect on the manifestation of biological activity. Hence, precipitation of sulfur by water during the synthesis and the equal amount of the components were optimal conditions for obtaining of the S/AgI microstructures with antimicrobial action.

Conclusion

S/AgI microstructures were prepared by solvothermal DMSO-mediated synthesis using two methods of sulfur precipitation: at room temperature (method 1) and by water (method 2). The samples were represented by the next percentages of AgI: 10, 30 and 50 %.

XRD and Raman spectroscopy revealed that all samples contain sulfur and AgI. According to EDS elemental mapping, sulfur is present in the form of both large and small grains. The large grains are covered by a thin layer of AgI. SEM results have shown that sulfur have irregular shape for both methods of synthesis. As for a size particles, first synthesis method produced sulfur with greater size (20-50 μm). AgI particles have triangular and hexagonal shape. 10 % samples represented by AgI size range from 0.5 to 3 μm , 30 % – from 0.2 to 0.3 μm , 50 % – from 1 to 3 μm . The second method yielded sulfur particles with size from 5 to 20 μm . The size of the AgI particles was the next: 10 % – 0.3 – 0.9 μm ; 30 % – 0.4 – 1 μm ; 50 % – 0.5 – 2 μm . The morphology of AgI particles is represented by non-defined shape. In general, method 1 gives larger particles of sulfur in comparison with method 2.

The potential application of the S/AgI (1, 2) 10, 30 and 50 % in the photocatalysis was not confirmed, as neither of the samples was able to degrade molecules of Orange II under visible light irradiation. The kinetics of the photocatalytic process was accepted as a pseudo-first-order reaction.

Biological activity was studied on the six types of the test strains. Only S/AgI (2) 50 % was able to inhibit test strains of *S. aureus* ATCC BAA-39, *P. aeruginosa* ATCC 9027 and *Erwinia amylovora* at MBC/MFC 5000 $\mu\text{g/mL}$, and *E. coli* ATCC 8739 at 2500 $\mu\text{g/mL}$. The manifestation of biological activity by only one sample can be explained by the formation of a bond between sulfur and AgI. Thus, the precipitation of sulfur with water and a 50 % content of sulfur and AgI are optimal for obtaining microstructures with the ability to suppress certain microorganisms.

Acknowledgements

This work was financially supported by scientific project of Ministry of Education and Science of Republic of Kazakhstan AP08855868 and done on state assignment of IGM SB RAS.

References

1. Singh R.P., Singh P., Singh K.R. (2021) Introduction to Composite Materials: Nanocomposites and their Potential Applications. Composite Materials CRC Press, 28 p. ISBN 9781003080633
2. Jaspal D., Malviya A. (2020) Composites for wastewater purification: A review. *Chemosphere*, vol. 246, pp. 125788. <https://doi.org/10.1016/j.chemosphere.2019.125788>
3. Egbo, M. K. (2021). A fundamental review on composite materials and some of their applications in biomedical engineering. *J King Saud Univ Eng Sci*, vol. 33, no. 8, pp. 557-568. <https://doi.org/10.1016/j.jksues.2020.07.007>
4. Xu X., Ye S., Liu S., Yan T. (2021). Silver Iodide as a Host Material of Sulfur for Li-S Battery. *J Electrochem Soc*, vol. 168, no. 6, pp. 060536 <https://doi.org/10.1149/1945-7111/ac0bf2>
5. Velmurugan S., Balu S., Palanisamy S., Yang T. C. K., Velusamy V., Chen S. W., El-Shafey E. S. I. (2020). Synthesis of novel and environmental sustainable AgI-Ag₂S nanospheres impregnated g-C₃N₄ photocatalyst for efficient degradation of aqueous pollutants. *Appl Surf Sci*, vol. 500, pp. 143991 <https://doi.org/10.1016/j.apsusc.2019.143991>
6. Shankar S., Jaiswal L., Rhim J. W. (2021) New insight into sulfur nanoparticles: Synthesis and applications. *Crit Rev Environ Sci Technol*, vol. 51, no. 20, pp. 2329-2356. <https://doi.org/10.1080/10643389.2020.1780880>
7. Chen W., Qian T., Xiong J., et. al. (2017) A new type of multifunctional polar binder: toward practical application of high energy lithium sulfur batteries. *Adv mater*, vol. 29, no. 12, pp. 1605160. <https://doi.org/10.1002/adma.201605160>
8. Zeng L., Wang N., Yang J., et. al. (2017) Application of a sulfur cathode in nucleophilic electrolytes for magnesium/sulfur batteries. *J Electrochem Soc*, vol. 164, no. 12, pp. A2504. <https://doi.org/10.1149/2.1131712jes>
9. Barce Ferro C. T., Dos Santos B. F., da Silva C. D., et. al. (2020) Review of the syntheses and activities of some sulfur-containing drugs. *Cur Org Synt.*, vol. 17, no. 3, pp.192-210. <https://doi.org/10.2174/1570179417666200212113412>
10. Valle S. F., Giroto A. S., Klaic R., et.al. (2019) Sulfur fertilizer based on inverse vulcanization process with soybean oil. *Polym degrad stab*, vol. 162, pp. 102-105. <https://doi.org/10.1016/j.polymdegradstab.2019.02.011>

11. Kim Y. H., Kim G. H., Yoon K. S., et. al. (2020) Comparative antibacterial and antifungal activities of sulfur nanoparticles capped with chitosan. *Microb Pathog*, vol. 144, pp. 104178. <https://doi.org/10.1016/j.micpath.2020.104178>
12. Saedi S., Shokri M., Rhim J. W. (2020) Antimicrobial activity of sulfur nanoparticles: Effect of preparation methods. *Arab J Chem*, vol. 13, no. 8, pp. 6580-6588. <https://doi.org/10.1016/j.arabjc.2020.06.014>
13. Ahmad N., Alshehri A. M., Khan, Z. R., et. al. (2022) Tailoring of band gap, dielectric and antimicrobial properties of silver iodide nanoparticles through Cu doping. *Mater Sci Semicond Process*, vol. 137, pp. 106239. <https://doi.org/10.1016/j.mssp.2021.106239>
14. Wang K., Li Q., Liu B., et. al. (2015) Sulfur-doped g-C₃N₄ with enhanced photocatalytic CO₂-reduction performance. *Appl Catal B*, vol. 176, pp. 44-52. <https://doi.org/10.1016/j.apcatb.2015.03.045>
15. Chen L., Zhu D., Li J., et. al. (2020) Sulfur and potassium co-doped graphitic carbon nitride for highly enhanced photocatalytic hydrogen evolution. *Appl Catal B*, vol. 273, pp. 119050. <https://doi.org/10.1016/j.apcatb.2020.119050>
16. Wen X. J., Shen C. H. Fei, et. al. (2020) Recent developments on AgI based heterojunction photocatalytic systems in photocatalytic application. *Chem Eng J*, vol. 383, pp. 123083. <https://doi.org/10.1016/j.cej.2019.123083>
17. Li J., Liu B., Han X., et.al. (2021) Direct Z-scheme TiO₂-x/AgI heterojunctions for highly efficient photocatalytic degradation of organic contaminants and inactivation of pathogens. *Sep Purif Tech*, vol. 261, pp. 118306. <https://doi.org/10.1016/j.seppur.2021.118306>
18. Soltaninejad V., Ahghari M. R., Taheri-Ledari R., Maleki A. (2021) Bifunctional PVA/ZnO/AgI/Chlorophyll Nanocomposite Film: Enhanced Photocatalytic Activity for Degradation of Pollutants and Antimicrobial Property under Visible-Light Irradiation. *Langmuir*, vol. 37, no 15, pp. 4700-4713. <https://doi.org/10.1021/acs.langmuir.1c00501>
19. Rehan M., Khattab T. A., Barohum A., et al. (2018) Development of Ag/AgX (X= Cl, I) nanoparticles toward antimicrobial, UV-protected and self-cleanable viscose fibers. *Carbohydr polym*, vol. 197, pp. 227-236. <https://doi.org/10.1016/j.carbpol.2018.06.010>
20. Jiang X., Ma Y., Zhao C., et. al. (2018) Synthesis of flower-like AgI/Bi₅O₇I hybrid photocatalysts with enhanced photocatalytic activity in rhodamine B degradation. *J of Mater Res*, vol. 33, no. 16, pp. 2385-2395. <https://doi.org/10.1557/jmr.2018.201>
21. Yuan D., Huang L., Li Y., et. al. (2020) A novel AgI/BiOI/pg-C₃N₄ composite with enhanced photocatalytic activity for removing methylene orange, tetracycline and *E. coli*. *Dyes Pigm*, vol. 177, pp. 108253. <https://doi.org/10.1016/j.dyepig.2020.108253>
22. Li Q., Wang K., Lu X., et. al. (2020) In situ synthesis of AgI/SnS₂ heterojunction photocatalysts with superior photocatalytic activity. *Int J Electrochem Sci*, vol. 15, pp. 9256-9270. doi: 10.20964/2020.09.77
23. Ujjan Z. A., Bhatti M. A., Shah A. A., et. al. (2022) Simultaneous doping of sulfur and chloride ions into ZnO nanorods for improved photocatalytic properties towards degradation of methylene blue. *Ceram Int*, vol. 48, no. 4, pp. 5535-5545. <https://doi.org/10.1016/j.ceramint.2021.11.098>
24. Shao-you L., Yuan-dao C., Tao-yu Q., et. al. (2018) Sulfur doped lead monoxide superfine powder materials: solid-state synthesis, characterization, adsorption and photocatalytic property of methylene blue. *J Inorg and Organomet Polym Mater*, vol. 28, no. 6, pp. 2584-2595. <https://doi.org/10.1007/s10904-018-0942-4>
25. Madruga G. M., Crivellenti L. Z., Borin-Crivellenti S., et. al. (2017) Comparative use of dimethyl sulphoxide (DMSO) in different animal species. *Vet Med (Praha)*, vol. 62, no. 4, pp. 179-185. doi: 10.17221/176/2015-VETMED
26. Tashrifi Z., Khanaposhtani M. M., Larijani B., Mahdavi M. (2020) Dimethyl Sulfoxide: yesterday's solvent, today's reagent. *Adv Synth Catal*, vol. 36, no. 1, pp. 65-86. <https://doi.org/10.1002/adsc.201901021>
27. Khademian M., Zandi M., Amirhoseiny M., Dorrani D. (2017) Synthesis of CuS nanoparticles by laser ablation method in DMSO media. *J Clust Sci*, vol. 28, no. 5, pp. 2753-2764. <https://doi.org/10.1007/s10876-017-1257-2>
28. Borreguero A. M., Rodríguez J. F., Velencoso M. M., et. al. (2019) DMSO as solvent on the synthesis of flame-retardant polyether polyols. *J Appl Polym Sci*, vol 136, no. 6, pp. 47042. <https://doi.org/10.1002/app.47042>
29. Burkitbayev, M. M., Urakaev, F. Kh. (2020) Temperature dependence of sulfur solubility in dimethyl sulfoxide and changes in concentration of supersaturated sulfur solutions at 25° C. *J Mol Li*, vol. 316, p. 113886. <https://doi.org/10.1016/j.molliq.2020.113886>

30. Khan N. V., Burkitbayev M. M., Urakaev F. Kh. (2019) Preparation and Properties of Nanocomposites in the Systems S-AgI and S-Ag₂S-AgI in Dimethyl Sulfoxide. *Mater Sci Eng*, vol. 704, no. 1, pp. 012007). doi:10.1088/1757-899X/704/1/012007
31. Khan, N. V. (2022). Synthesis of the S/AgBr nano/micropowder in DMSO-water system. *Chem Bull Kaz Nat Univ*, vol. 104, no. 1, pp. 4-10
32. CLSI standard M07 (2018) Methods for Dilution Antimicrobial Susceptibility Tests for Bacteria That Grow Aerobically; 11th ed. Wayne, PA, USA.
33. CLSI standard M27 (2017) Reference Method for Broth Dilution Antifungal Susceptibility Testing of Yeasts. 4th ed. Wayne, PA, USA.
34. Cui L., Jiao T., Zhang Q., et. al. (2015) Facile preparation of silver halide nanoparticles as visible light photocatalysts. *Nanomater Nanotechnol*, vol. 5, pp. 20. <https://doi.org/10.5772/60910>
35. McEvoy J. G., Cui W., Zhang Z. (2014) Adsorption and visible light degradation of methyl orange by Ag/AgCl-activated carbon composites. Carbon-enhanced photocatalysts for visible light induced detoxification and disinfection, 85.

© This is an open access article under the (CC)BY-NC license (<https://creativecommons.org/licenses/by-nc/4.0/>). Funded by Al-Farabi KazNU